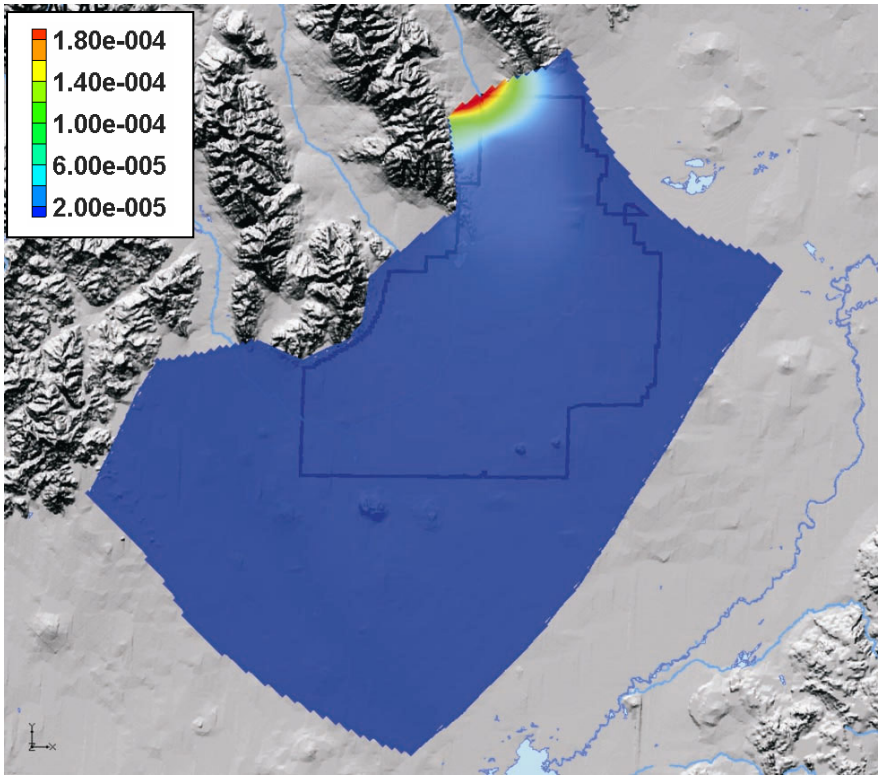

Figure 3-29. Sensitivity of the simulated heads to the underflow rate of the Birch Creek drainage basin.

of the Big Lost River and Birch Creek drainage basins. Visual comparison of these sensitivity maps also indicates that the simulated heads inside the INL Site boundaries, particularly the heads in the southern portion of the site, are relatively insensitive to the underflow rates. More importantly, these heads are almost equally sensitive to all three underflow rates. This has an important implication for the future transport simulations: the uncertainties associated with the flux estimates will not affect (or propagate to) transport predictions, because the simulated heads inside the INL Site, particularly in the southern portion of the site, will rise or fall in a uniform way when the estimated fluxes increase or decrease.

As shown in Figure 3-29, the simulated heads in the northern portion of the INL Site, particularly in the TAN area (or WAG 1), are more sensitive to the underflow rate of the Birch Creek drainage basin than are the heads in the southern portion of the site. However, the simulated heads in the southern portion of the site are almost equally sensitive to the underflow rate of the Birch Creek drainage basin.

To more quantitatively investigate the sensitivity of the underflow rates to the simulated heads inside the INL Site boundaries, we present Table 3-4, which shows the sensitivity coefficient of the heads at the approximate centers of all nine INL Site facility areas. The numbers in this table are consistent with the previous sensitivity maps and support our previous conclusions regarding the sensitivity of the underflow rates.

3.1.10.3 Study of Sensitivity to the Precipitation Recharge. In the current two-dimensional flow model, a uniform precipitation recharge rate of 1.95×10^{-5} m/d (6.39×10^{-5} ft/d) was applied to the entire domain. This subsection presents the results of the sensitivity study on the precipitation rate.

We focus on the heterogeneous infiltration scenario by correlating the infiltration rate with the surface soil/rock types and record the changes of the simulated heads. Figure 3-30 shows the surface

Table 3-4. The sensitivities of heads at the facility centers to the underflow rates.

	WAG 1 (TAN)	WAG 2 (RTC)	WAG 3 (INTEC)	WAG 4 (CFA)	WAG 5 (PBF/ARA)	WAG 6 (EBR/BORAX)	WAG 7 (RWMC)	WAG 8 (NRF)	WAG 9 (MFC)
Big Lost River	2.64e-6	8.75e-6	8.65e-6	8.83e-6	8.51e-6	1.0e-5	1.1e-5	7.75e-6	6.56e-6
Little Lost River	1.1e-5	1.6e-5	1.6e-5	1.5e-5	1.5e-5	1.4e-5	1.4e-5	1.8e-5	1.4e-5
Birch Creek	1.5e-5	6.0e-6	5.95e-6	5.78e-6	5.76e-6	5.27e-6	5.12e-6	6.59e-6	5.91e-6

CFA = Central Facilities Area
EBR/BORAX = Experimental Breeder Reactor/Boiling Water Reactor Experiment
INTEC = Idaho Nuclear Technology and Engineering Complex
MFC = Materials and Fuels Complex
NRF = Naval Reactors Facility
PBF/ARA = Power Burst Facility/Auxiliary Reactor Area
RTC = Reactor Technology Complex
RWMC = Radioactive Waste Management Complex
TAN = Test Area North

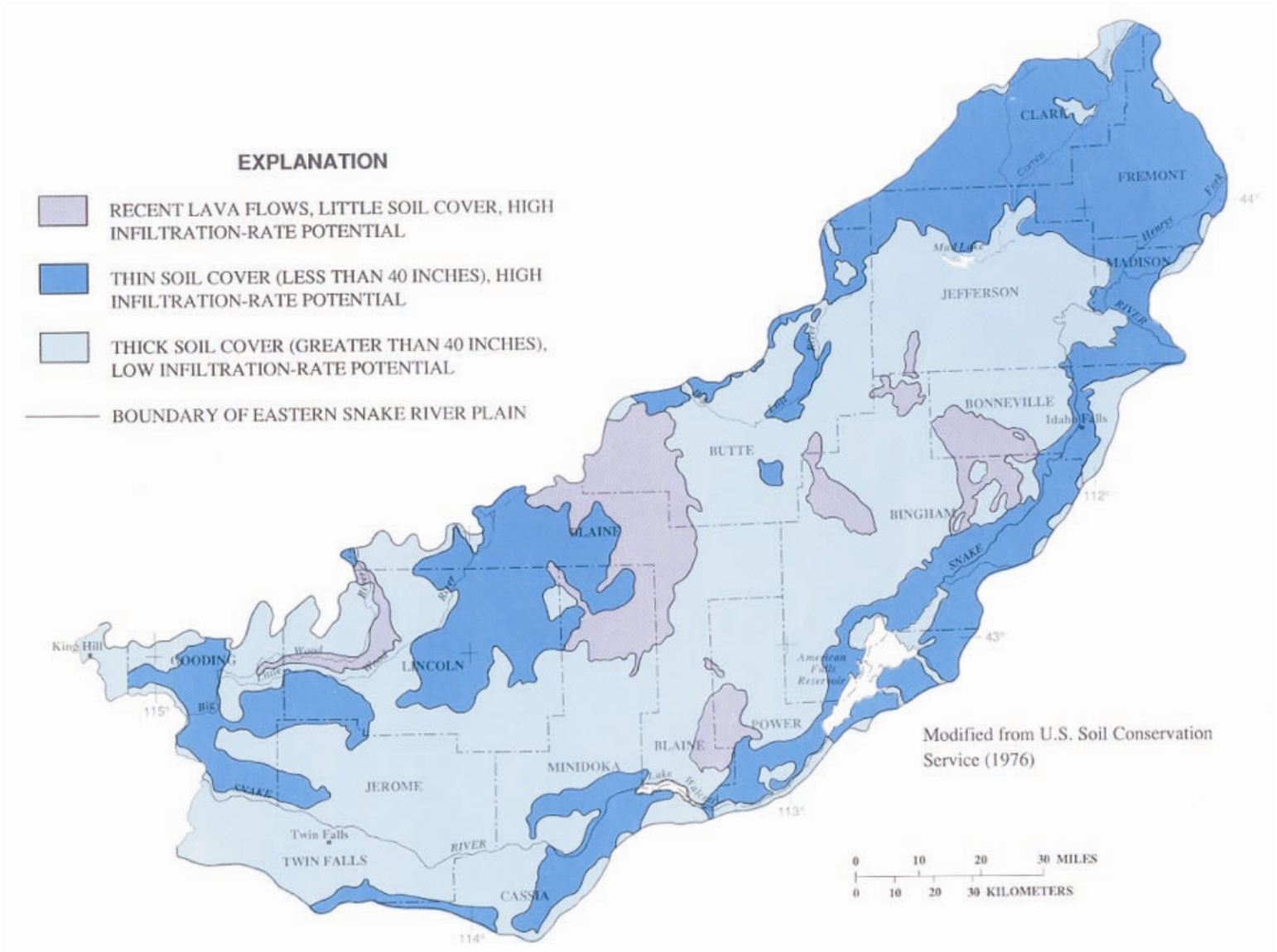

Figure 3-30. Surface soil/rock distribution map across the Snake River Plain.

soil/rock distribution across the entire Snake River Plain, which was used to derive the precipitation infiltration rates for Garabedian's (1992) flow model and the IWRRI model (IWRRI 2005). On the basis of the surface soil/rock distribution, we developed a heterogeneous precipitation infiltration rate map as show in Figure 3-31. The heterogeneous infiltration rate scenario was implemented in the two-dimensional model, and the head change for each grid block was calculated to evaluate the sensitivity of the simulated heads to the infiltration rate heterogeneity. Figure 3-32 shows the changes of simulated heads between the heterogeneous infiltration scenario and the homogeneous infiltration scenario.

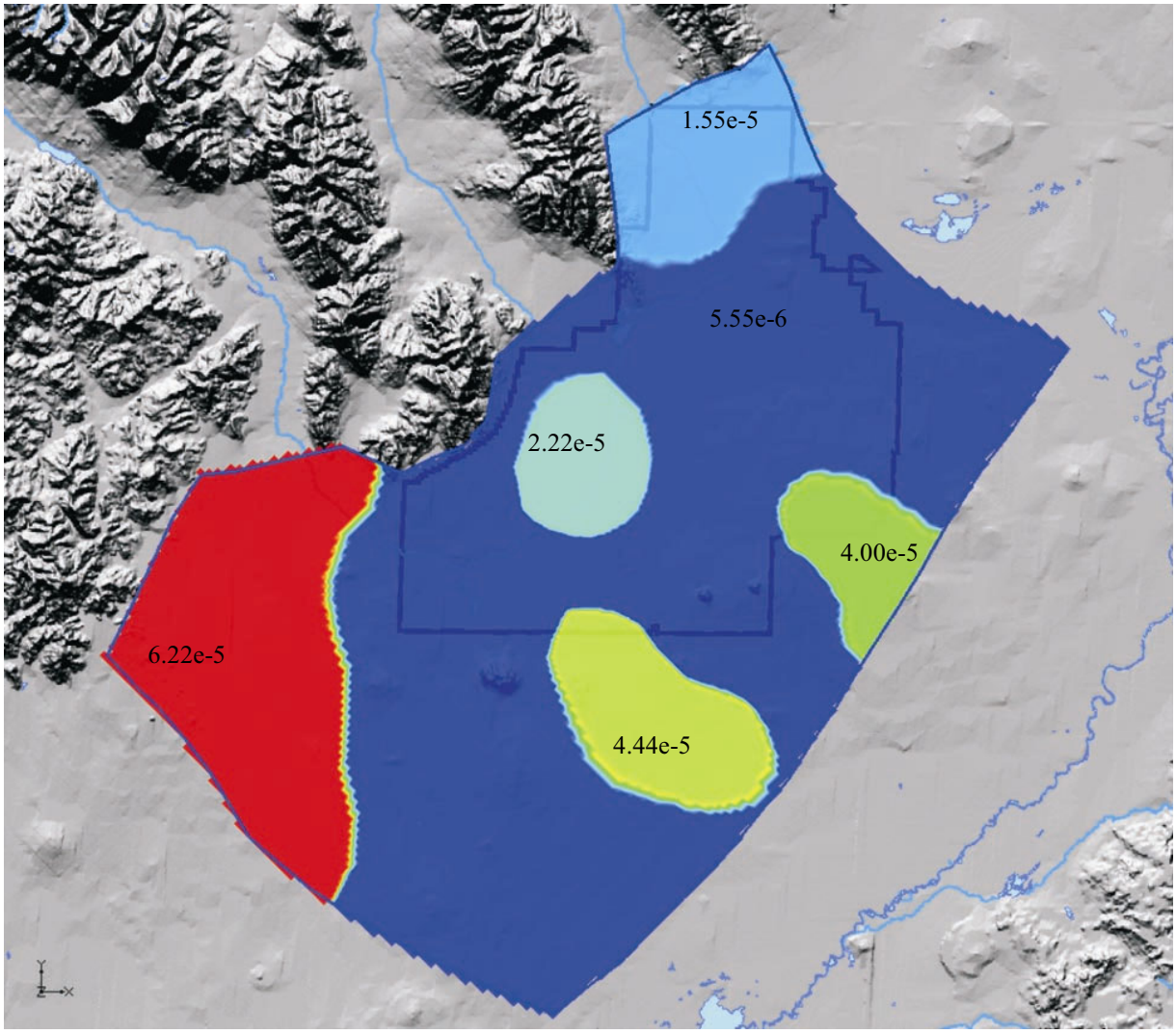

Figure 3-31. The heterogeneous precipitation infiltration rate (m/d) implemented in the two-dimensional model domain for sensitivity study.

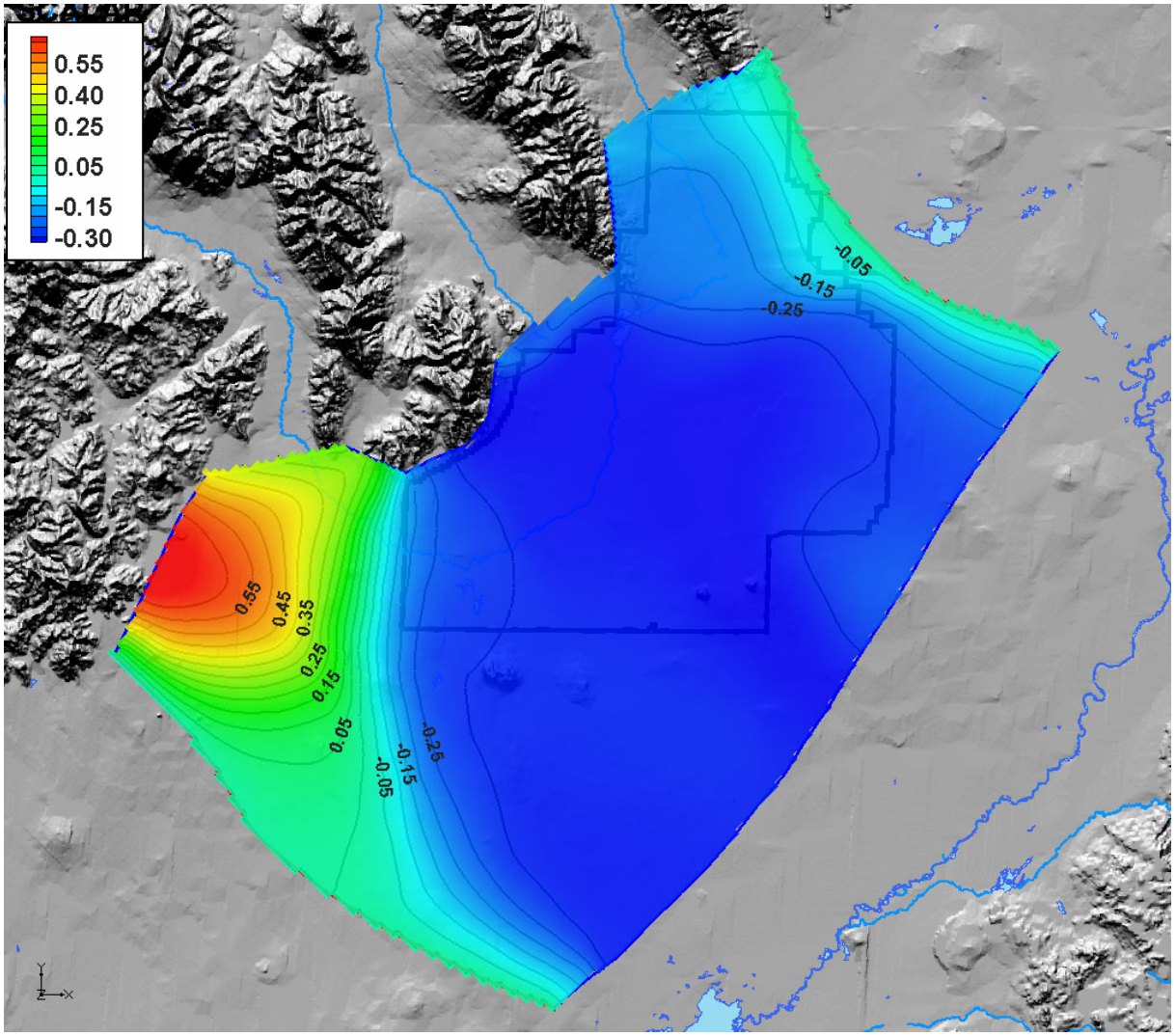

Figure 3-32. Changes (in meters) of simulated heads between heterogeneous and homogeneous infiltration scenarios.

Sensitivities of the simulated heads were highest in the southwestern part of the model domain, where the highest heterogeneous infiltration rate was used. Sensitivities of the simulated heads were lowest in the middle of the domain, where a small infiltration rate of 5.55e-6 m/d (1.8e-6 ft/d) was applied to a large portion of the model domain. However, the maximum absolute change of the simulated heads for both infiltration scenarios was only about 0.6 m (2 ft), still within the acceptance range of the simulation residuals (1 m [3.3 ft]). More importantly, the changes of heads inside the INL Site boundary, particularly changes in the southern portion of the site, are fairly uniform, as manifested by the large separation distance between the contour lines of head changes. This is particularly important for transport simulation, because such uniform changes of heads will not affect the gradient.

3.1.10.4 Particle Tracking Simulation of the Potential Contaminant Travel Paths. To further evaluate the potential travel paths of possible contaminants initiated from individual facilities, we conducted particle tracking simulations by using our two-dimensional simulated flow field. We considered both thick and thin aquifer scenarios and compared the particle tracking simulation results using the simulated head fields as input from both the zonation approach and pilot-point approach,

respectively. Figures 3-33 and 3-34 show the possible flow paths of contaminants initiated from some facilities. One interesting point is that the flow field calibrated by the pilot-point approach provides more realistic travel paths than does the zonation approach. In particular, the predicted travel path initiated from INTEC by the pilot-point approach is more consistent with the measured plume spreading. This result clearly demonstrates the need to accurately reproduce the flow field at both large and local scales in order to make reliable transport predictions.

An interesting result shown in Figures 3-33 and 3-34 is that the simulated travel paths are not necessarily consistent with the flow paths inferred from geochemical and isotope studies, as shown in Figure 2-32, where the inferred flow path from INTEC is more southeasterly. The simulated travel path from INTEC is more southerly.

Although the Figures 3-33 and 3-34 show the potential travel paths of contaminants, the travel paths have no information available with respect to travel time. In order to accurately depict and predict contaminant transport, a truly three-dimensional model is needed.

3.1.11 Limitations of the Two-dimensional Flow Model

The objectives of developing the current two-dimensional flow model are to better understand both the regional- and local-scale features, investigate the validity of various calibration approaches, and investigate the feasibility of using all aquifer wells available inside the INL Site boundaries and the rest of the model domain as calibration wells. The two-dimensional modeling results (primarily the pilot-point approach) are satisfactory in terms of meeting the above objectives.

Although we have used variable thickness, the two-dimensional model assumes the hydraulic conductivity and head are the same along the vertical direction. So the estimated hydraulic conductivity field and simulated head are the averages across the entire aquifer thickness. However, there is strong evidence that the vertical heterogeneity of the aquifer could lead to potential vertical flow within the system. Vertical flow will have important impacts on subsequent contaminant transport predictions. Where significant vertical flow exists in the aquifer, the two-dimensional flow model is inadequate for simulating transport.

Another limitation of the steady-state two-dimensional model is that it does not consider the dynamic nature of aquifer recharge (e.g., wet and drought periods). The model only considers a snapshot in time for its calibration. Calibrating flow ***and*** transport to long-term anthropogenic plumes and stable-isotope geochemistry plumes will be accomplished during the next phase of the OU 10-08 modeling project. The remainder of this subsection discusses limitations of a vertically integrated two-dimensional model for simulating transport.

First and foremost, transport is inherently three-dimensional within the aquifer. Contaminants from the vadose zone are introduced to the top of the aquifer and then begin mixing vertically along flow paths. In addition, contaminants are injected at depth. A two-dimensional model assumes constant concentration across the entire thickness of the aquifer, implying that whenever contaminant flux enters into the aquifer across the water table, the contaminants immediately mix (or dilute) along vertical directions within the whole aquifer. This assumption leads to significantly underestimated simulated contaminant concentrations within the aquifer.

Another limitation of the two-dimensional model is its inability to reproduce the “preferential” flow path identified through geochemical and isotope studies in the INL Site. This is based on the observations described in Subsection 3.1.10.4 regarding the divergence between simulated flow paths from INTEC compared to flow paths interpreted from sparse geochemical data. One hypothesis is that

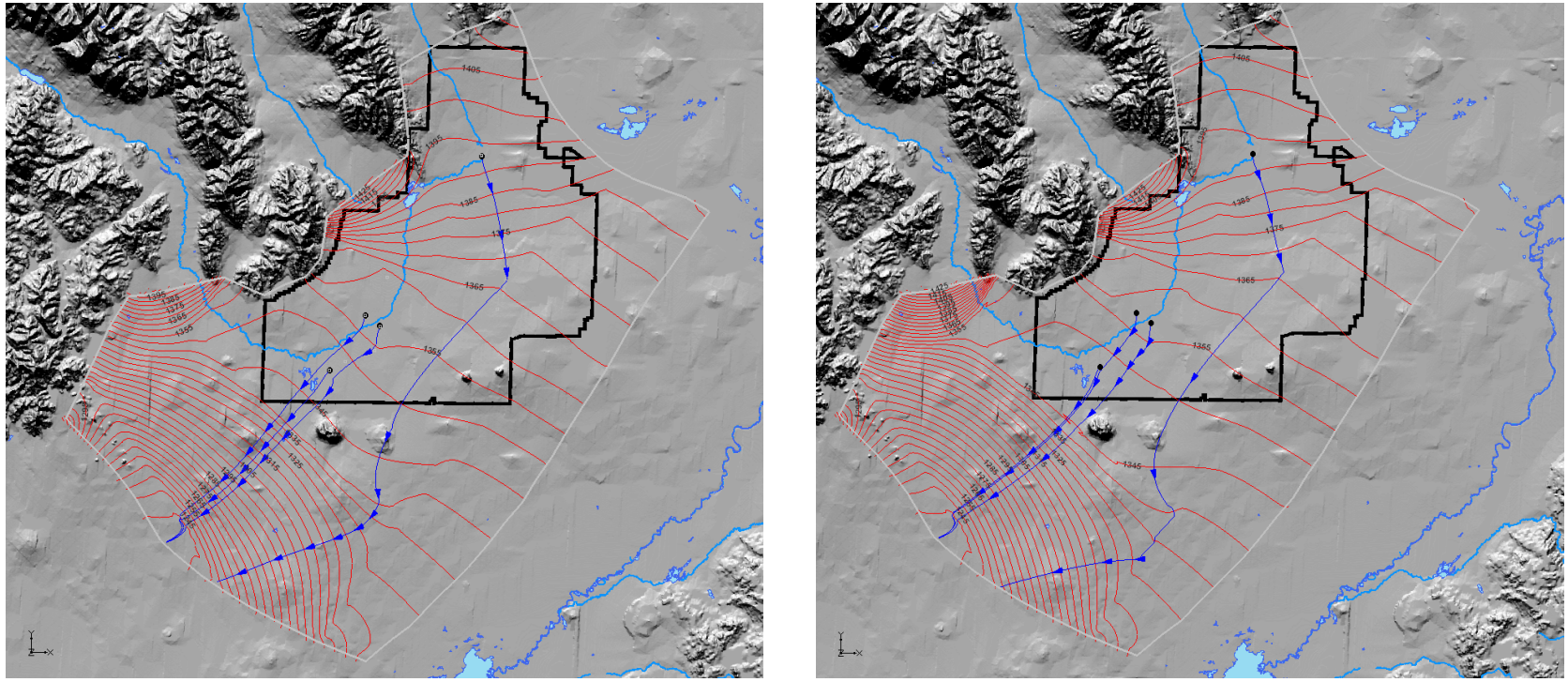

Figure 3-33. Simulated flow paths from individual WAGs using the head field calibrated by the zonation approach for the thick scenario (left) and the thin scenario (right).

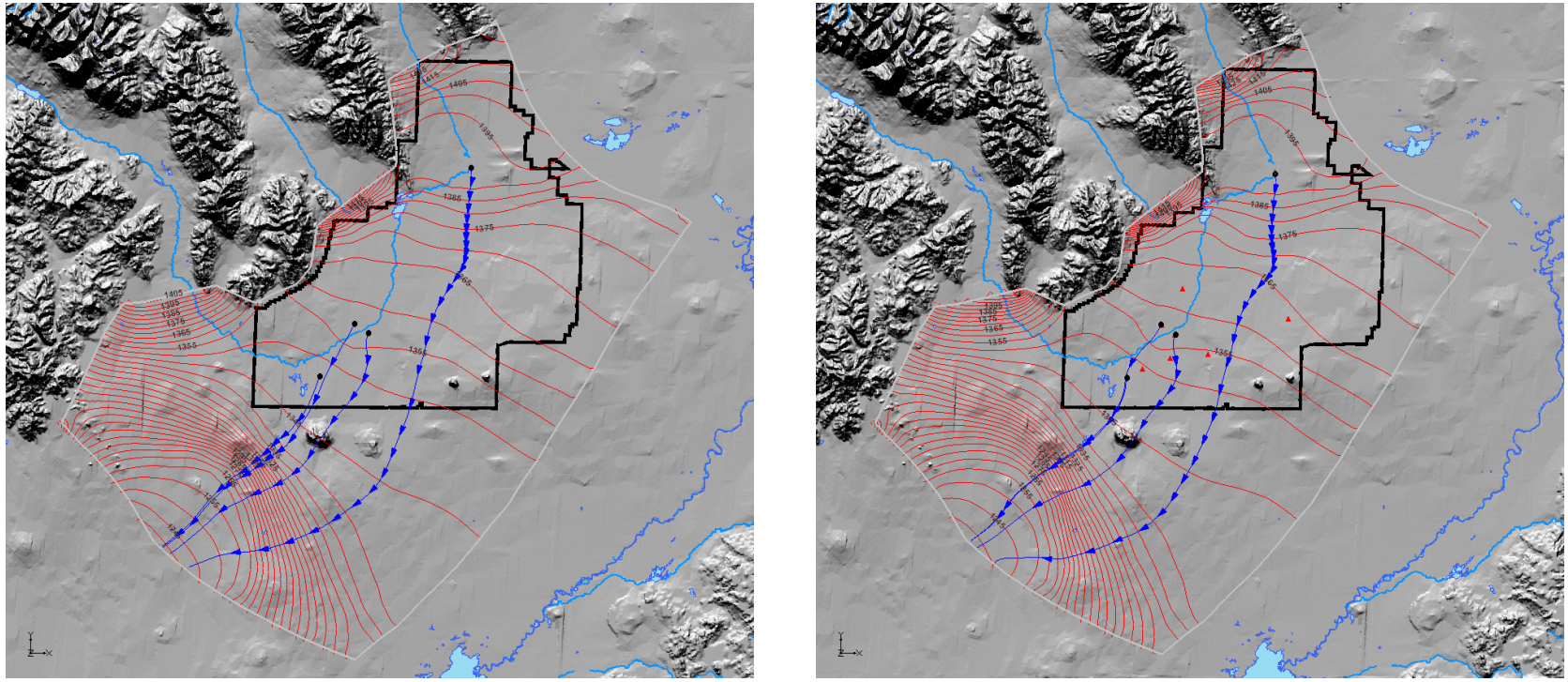

Figure 3-34. Simulated flow paths from individual WAGs using the head field calibrated by the pilot-point approach for the thick scenario (left) and the thin scenario (right).

this preferential flow path might be a feature only within the upper portion of the aquifer. A two-dimensional model can only address the lumped (averaged) effect across the entire thickness of the aquifer. A three-dimensional model is required to test this hypothesis by incorporating vertical heterogeneity. If the preferential flow exists, it will lead to much faster contaminant transport than we expected, and a three-dimensional model is required to test this hypothesis.

Due to the limitations of the two-dimensional flow model, we conclude that a fully three-dimensional model that incorporates both horizontal and vertical heterogeneities at various scales is required in order to accurately depict and predict the contaminant transport in the SRPA.

3.2 Thermo-hydraulic Two-dimensional Modeling Activities

The reliability of a flow and transport model relies entirely on its ability to mimic the system it represents. Thus, confidence in a model depends on how well it reproduces observed behavior. In general, the process of refining a model to match different sets of observations is termed calibration, and calibration to several data sets is preferred. In the SRPA, one of the calibration targets is the abundant temperature data available from boreholes and wells. Accordingly, a groundwater heat flow modeling study is being conducted to provide a quantitative means of relating observed groundwater temperature distribution to groundwater flow. Results of this effort will be used to constrain aquifer properties in a refined model calibration effort. A three-dimensional thermal model, calibrated to the areal and vertical distribution of subsurface temperature, is planned for completion in fiscal year 2006.

One of the principal questions that can be addressed via heat flow modeling is related to the isothermal nature of temperature profiles in the active portion of the aquifer. The homogenization of temperature in those sections clearly represents either significant vertical mixing or a horizontal rate of groundwater movement sufficiently fast to prevent significant heating from below. Vertical mixing may be occurring via vertical flow or via dispersion transverse to the principal direction of groundwater flow. Vertical flow, in turn, may be driven by pressure gradients or by free convection if temperature gradients are large enough to create significant buoyant forces.

The potential for free convection in groundwater systems can be assessed by calculating the Rayleigh number, a dimensionless number that essentially represents the ratio of buoyant forces, promoting vertical flow, to viscous and diffusive forces that inhibit vertical flow. The Rayleigh number, N_{Ra}, is as follows:

$$N_{Ra} = \frac{g \cdot \rho_0 \cdot c_w \cdot \rho_w \cdot L \cdot k \cdot \alpha_w \cdot \Delta T}{\mu_w \cdot \kappa_{eff}} \tag{3-1}$$

where

g	=	gravitational acceleration constant
ρ_0	=	water density at a specified background temperature
c_w	=	the specific heat of water
ρ_w	=	water density
L	=	aquifer thickness
k	=	intrinsic permeability
α_w	=	coefficient of volume expansion
ΔT	=	temperature difference across the system
μ_w	=	dynamic viscosity of water
k_{eff}	=	effective thermal conductivity.

Theoretical analysis indicates that free convection in groundwater does not occur until the Rayleigh number exceeds ~40 (Lapwood 1948). To estimate the potential for free convection in the eastern SRPA, we can thus determine whether the estimated Rayleigh number for the system exceeds that value. Assuming a temperature gradient similar to that observed in the subaquifer at the Middle-1823 well (~0.07°C m^{-1}), and assuming an aquifer thickness (L in Equation 3-1) of 200 m (~656 ft), the potential temperature difference across the system, ΔT, is about 13°C. Under these assumptions, the Rayleigh number depends primarily on the intrinsic permeability, k, of the system. Based on estimates of Ackerman (1991), the transmissivity of the SRPA ranges from 0.1 to 70,606 m^2 day^{-1} (1.1 to 760,000 ft^2 day^{-1}). Again, assuming an aquifer thickness of ~200 m (656 ft) implies that the intrinsic permeability of the aquifer ranges from approximately < 10^{-15} to 10^{-10} m^2. The Rayleigh number for that k range is then readily calculated by assuming that other variables in Equation 3-1 vary little from their values at ~15°. Results indicate that free convection is possible but unlikely, because the combination of temperature and permeability provides the necessary conditions only at the maximum estimated permeability for the system (Figure 3-35).

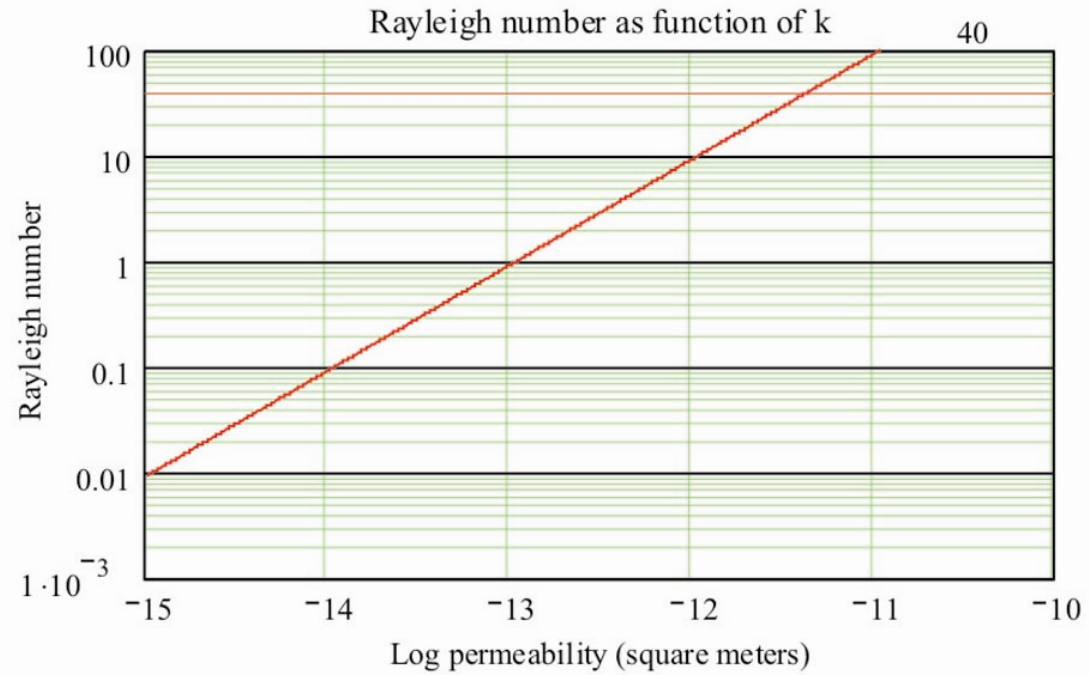

Figure 3-35. Rayleigh number versus intrinsic permeability, k, for an assumed aquifer thickness of 200 m (656 ft) and temperature difference of ~13°C. The estimated range for k is based on transmissivity estimates of Ackerman (1991). The red line indicates the threshold value (~40) for free convection in groundwater (Lapwood 1948).

Other plausible mechanisms for producing the isothermal profiles in the aquifer are high horizontal groundwater velocities and strong mechanical dispersion in the vertical direction induced by flow in the horizontal plane. As a preliminary exploration of how these effects might be explored in a heat flow model, we conducted a set of simple modeling experiments with a two-dimensional block model scaled to reflect average dimensions of the eastern SRPA. Using MATLAB and the MATLAB PDE Toolbox, we constructed a three-layer model of the system comprised of a 200-m (656-ft) thick vadose zone, a 200-m (656-ft) thick aquifer, and a 100-m (328-ft) thick subaquifer (Figure 3-36). Assuming that groundwater flow and heat transport are uncoupled, the steady-state convection-dispersion equation that follows is solved for the entire system, with stratigraphic differences represented by differences in effective thermal

conductivity, advective velocity, and boundary conditions. The equations are solved using the finite element method, using the Gauss-Newton iteration to solve the prescribed non-linear set of elliptic equations.

$$\left[\frac{\partial}{\partial x}\left(k_{eff}\frac{\partial T}{\partial x}\right)+\frac{\partial}{\partial y}\left(k_{eff}\frac{\partial T}{\partial y}\right)\right]-\left[\frac{\partial}{\partial x}\left(C_w q_x T\right)+\frac{\partial}{\partial y}\left(C_w q_y T\right)\right]=0 \qquad (3\text{-}2)$$

where the effective thermal conductivity, $\kappa_{eff,}$ is defined as

$$\kappa_{eff}=\kappa+\alpha_i q_x C_{eff} \qquad (3\text{-}3)$$

where

κ = thermal conductivity of the solid matrix
α_i = dispersivity, in direction i (longitudinal or transverse)
q_x = flux density of water in the x direction
C_{eff} = effective heat capacity of the solid/water matrix.

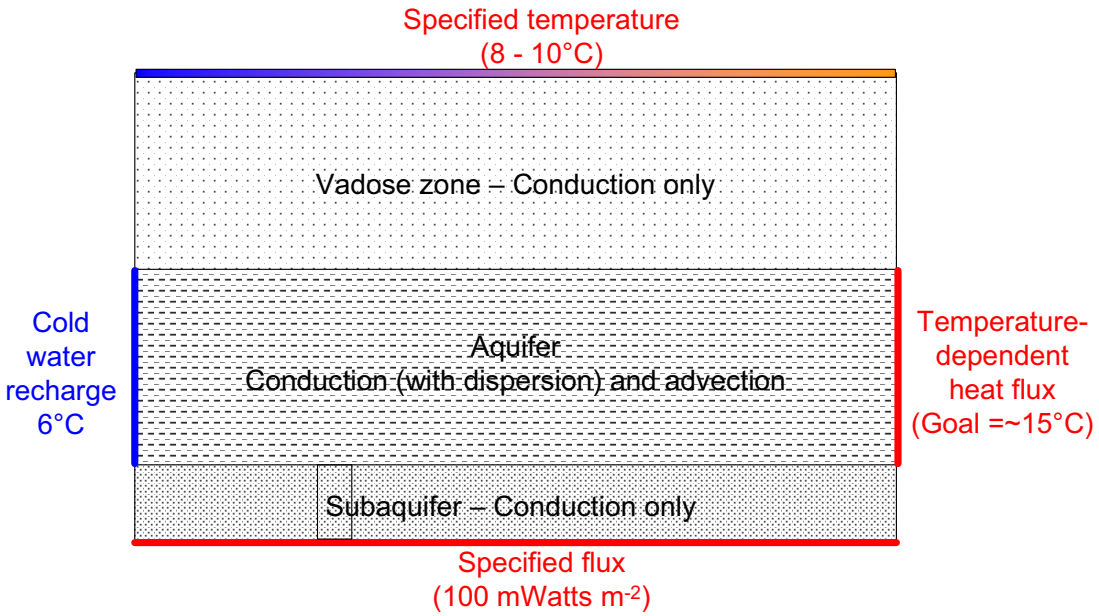

Figure 3-36. Schematic representation of the two-dimensional heat transport model.

We assumed a thermal conductivity of the solid/water matrix, κ, of 1.9 J m^{-1} sec^{-1} K^{-1}; an effective heat capacity, $C_{eff,}$ (solid + water), of 2.3×10^6 J m^{-3} K^{-1}; and a heat capacity for water, C_w, of 2.1×10^6 J m^{-3} K^{-1}. The flux density, q_x, was calculated from the average groundwater velocity assuming a porosity of 0.05. The dispersion coefficients, α_i, for dispersion of heat in the i directions are described below, and further details of notation and parameter values used in the calculations are included in Appendix B.

The model is designed to broadly represent a vertical cross section along a flowline through the ESRP, with flow from left to right. Thus, horizontal distance represents distance along a flow line extending from the edge of the Yellowstone Plateau to the Snake River near Thousand Springs,

approximately ~200 km (124 mi). This length is much greater than the thickness of the system. To scale the system appropriately, without requiring either a large number of elements or triangular elements with high aspect ratios, horizontal derivative terms in the equation matrices were multiplied by the appropriate constant.

In the aquifer layer, a uniform groundwater velocity of 3 m day^{-1} (~10 ft day^{-1}) is assumed. The advective term is zero in the other layers. A heat flux of 100 mWatts m^{-2} is specified along the bottom boundary of the system, and temperature along the top boundary is fixed, varying from 8°C on the left to 10°C on the right, representing ground temperatures on the ESRP. Temperature on the left, or recharge, boundary is fixed at 6°C, slightly colder than the overlying ground surface. The right, or discharge, boundary is a zero-gradient condition, so that the heat flux equals that advected across the boundary. All other boundaries are zero-flux boundaries.

In the eastern SRPA, temperatures along the discharge boundary are about 14 to 15ºC, and if the two-dimensional model described in this report adequately describes the geometry of the system and controls on heat flow in the system, the temperatures on the right-hand boundary of the model would be in that range. This model, however, is intended only to examine the basis sensitivity of the system to primary controls and should not be expected to accurately portray heat flow along a flow line to that level of detail. The discharge temperature is, therefore, provided only as a reference to illustrate how the model sensitivity to various parameters compares to the overall accuracy of the calculated temperature distribution. Note also that the temperatures specified along the boundaries do not exactly match observed ranges and are intended only to reflect the general trends within the system.

A base case simulation that includes longitudinal and transverse (vertical mixing) dispersivities of 1 m (3.3 ft) and 0.1 m (4 in.) describes a temperature distribution (Figure 3-37a) with several similarities to previous descriptions (Brott et al. 1981) of temperature trends along a flowline in the eastern SRPA. First, vertical temperature gradients in the recharge area are negative (temperature increasing with elevation), because the specified recharge temperature is colder than the mean annual air temperature at that location. Second, the flux of heat from below quickly effects a reversal in the vertical gradients, so that downstream (to the right) vertical gradients are positive and increasingly steeper with distance.

The modeled temperature distribution also exhibits several substantial differences from that observed in the SRPA. Near-isothermal vertical gradients exist only very near the recharge zone, for example, and little contrast exists in the gradient between the aquifer and subaquifer anywhere in the system. This contrasts markedly with the large difference in temperature gradient found between the active aquifer and subaquifer in wells that penetrate both systems. Discharge temperatures in this base case simulation (~25 to 30°C) are also considerably warmer than observed temperatures (approximately 15°C) at the recharge area. These differences suggest either that the included heat transport parameters (boundary conditions, thermal conductivities, advective velocity, and dispersivities) are incorrect or that this highly simplified model does not adequately capture the processes important to temperature control along a flowline through the aquifer. While the latter may be true, the sensitivity of the system to first-order heat flow processes should still be instructive, and we examine now how changes to some of these parameters affect the simulated temperature distribution.

Previous studies (Robertson 1974; Goode and Konikow 1990b) have indicated that longitudinal dispersivities in the system are on the order of 90 m (295 ft) in the aquifer beneath the INL Site. While large, dispersivity of that magnitude has only a minor effect (Figure 3-37b) on the large-scale temperature distribution here, primarily because the mixing scale is still relatively small compared to the length of the system, 200 km (124 mi). The advective velocity is an important control on the heat distribution, because it acts to alter the direction of heat transport from upward to sideways. In this system, the base case temperature distribution demonstrates that the advective velocity is insufficient to erase the effects of

heating along a flowline; temperatures increase by approximately 20°C across this system. A 5x increase in the advective velocity (Figure 3-37c) demonstrates that the system is quite sensitive to that velocity, and that temperature changes along a flowline might be diagnostic of velocity. The simulation also suggests that the observed nearly isothermal vertical profiles are not readily explained by the relatively fast advection in the system. In the base case scenario, vertical gradients across the aquifer are not much different than in the subaquifer, and the increase in velocity primarily acts to increase the gradient in both the subaquifer and aquifer, rather than increase the contrast between the two.

Vertical mixing within the aquifer could be the result of mechanical dispersion along a flowline. In the base case simulation, the transverse dispersivity is set to 0.1 m (3.3 ft), one tenth of the longitudinal dispersivity. If we again increase the longitudinal dispersivity to that estimated from previous studies, 90 m (295 ft), but also maintain the 10:1 ratio of longitudinal to transverse dispersivity, we see that the vertical gradients are very sensitive to that parameter (Figure 3-37d). In this example, temperature gradients in the aquifer are nearly isothermal along the entire flowline, and they contrast markedly with the underlying and overlying vertical gradients. This latter example demonstrates that the isothermal profiles commonly observed in SRPA wells might be excellent indicators of the degree of vertical mixing occurring along a flow path and thus provide a sound means of constraining longitudinal dispersivity in the system.

Note that the advantages gained from a better understanding of vertical mixing behavior might extend beyond those associated with constraining transport parameters. Development of a three-dimensional model for the SRPA requires a knowledge of the subsurface, and acquiring this knowledge can be very expensive to obtain. As discussed above, the isothermal temperature profiles suggest that vertical mixing in this system might be relatively rapid, and where vertical mixing is rapid, the system might well be described by a two-dimensional flow model. Thus, the temperature data might provide a robust means of identifying areas where the planned three-dimensional flow and transport model might reasonably assume homogeneity in the vertical direction and allow more focused effort on three-dimensional structure in areas with less pronounced vertical mixing.

One of the difficulties in parameterizing a heat flow model is that the geothermal heat flux is generally only roughly known. In the eastern SRPA, for example, results of an energy budget analysis of the system (Brott et al. 1981) indicate that the average geothermal heat flux is approximately 200 mWatt m^{-2}, while analysis of deep temperature profiles in the same region suggests that the flux is approximately 110 watts m^{-2}. Experiments with the two-dimensional model can provide insight to the sensitivity of temperature distribution to that value. As a simple example, doubling the heat flux across a 1-km (0.6-mi) length of the system has little impact on the temperature distribution (Figure 3-38), even near the bottom of the aquifer. This suggests that local hot spots in the temperature field might be the result of vertical movement of deep water, rather than simply variations in the underlying geothermal gradient.

3.3 Summary

The two-dimensional vertical profile model developed during the OU 10-08 two-dimensional modeling effort provides several insights as to how temperature data might be used to better constrain aquifer properties. First and foremost, the temperature data are one of the few parameters that have been obtained along the vertical dimension of the aquifer, and preliminary heat flow studies indicate that those temperature profiles can provide a quantitative means of constraining horizontal groundwater velocity and vertical mixing behavior.

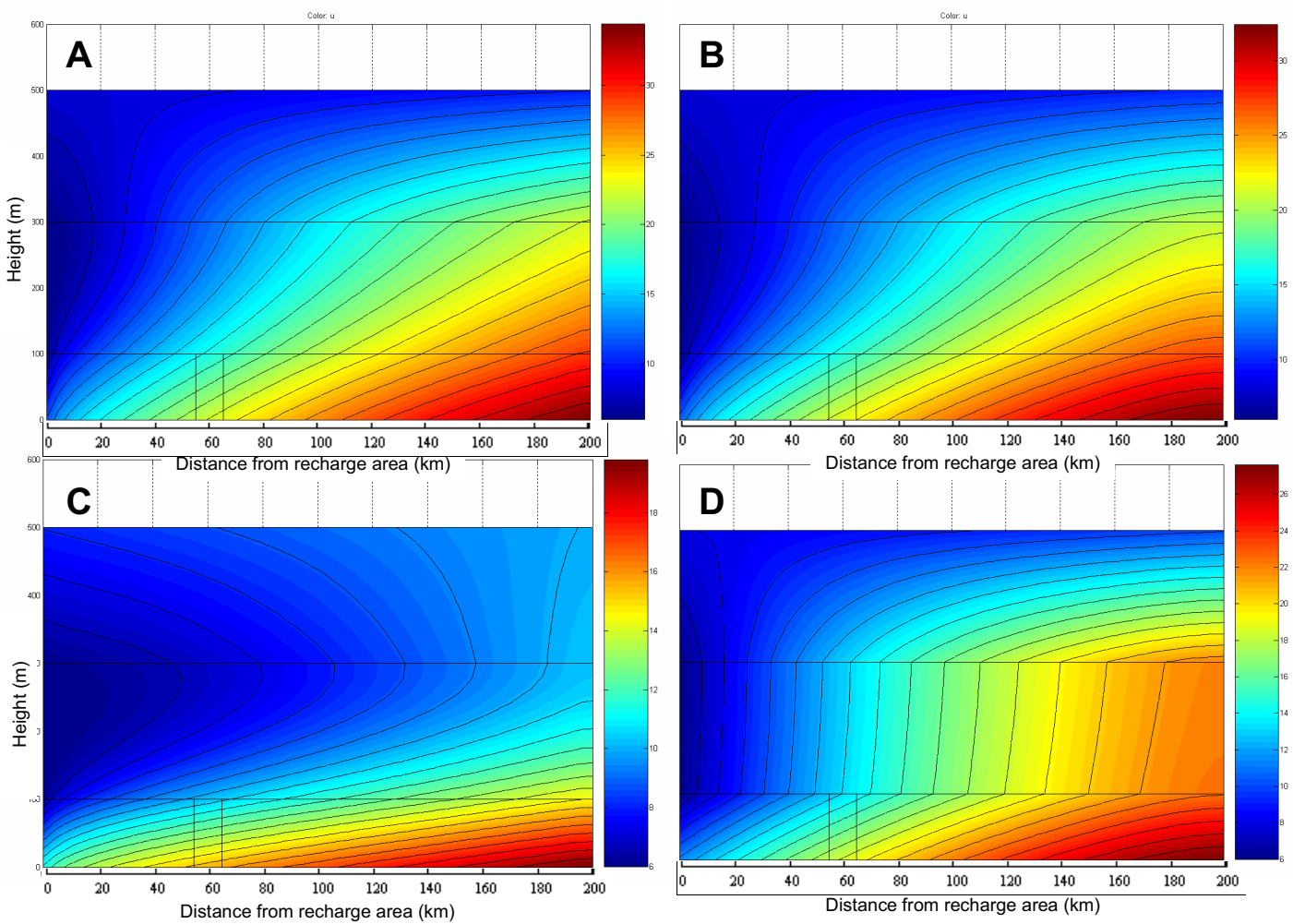

Figure 3-37. Simulated temperature distributions for the model depicted in Figure 3-36 for four scenarios described in the text: (a) simulated temperature distribution for the base case simulation described in the text, with α_L = 1 m, α_T = 0.1 m, ν = 3 m s^{-1}; (b) effect of increased longitudinal dispersivity on temperature distribution, base case condition with α_L = 90 m; (c) effect of a 5x increase in advective velocity, base case condition with ν = 15 m s^{-1}; and (d) effect of increased longitudinal dispersivity on temperature distribution, base case condition with α_L = 90 m and α_T = 9 m. Temperature scales are shown to the right of each plot. Vertical axes are meters, and horizontal axes are kilometers.

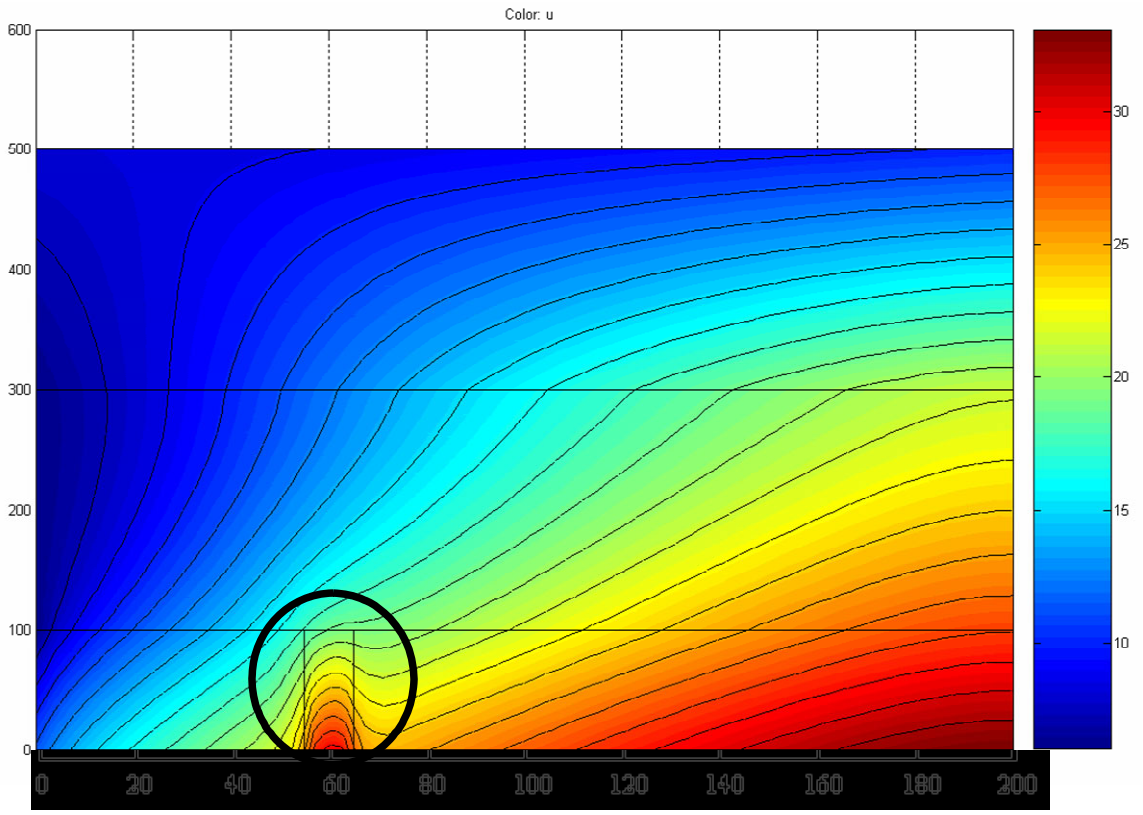

Figure 3-38. Simulated temperature distributions for the model depicted in Figure 3-36, for base case conditions, but with vertical heat flux doubled along the lower boundary of the circled rectangle.

In addition, the two-dimensional temperature distribution of the system is relatively well defined, the heat flux at the bottom of the aquifer can be obtained from approximately 10 deep wells, and the heat flux from the aquifer to the ground surface can be readily obtained at relatively high resolution. Thus, the preliminary heat flow studies conducted during fiscal year 2005 strongly support the argument that more detailed, three-dimensional heat flow modeling will greatly aid in constraining aquifer hydraulic properties, thereby providing increased confidence in predictions using the OU 10-08 groundwater flow and contaminant transport model.

Finally, the value of a heat flow study of the eastern SRPA is not limited to better constraining transport parameters. Preliminary results suggest that the nearly isothermal profiles commonly observed in deep boreholes might reflect strong vertical mixing that effectively results in vertically integrated transport behavior. Analysis of the temperature profiles might thus provide a means of identifying areas where the three-dimensional model might be considerably simplified to reflect, in essence, a homogeneous layered system.